Impact of Polylactide Fluorinated End-Group Lengths and Their Dynamics on Perfluorohexane Microcapsule Morphology

Guilherme Picheth, Laurence Moine, Sophie Houvenagel, Leociley Menezes, Guilherme L Sassaki, Camille Dejean, Nicolas Huang, Rilton Alves de Freitas, Nicolas Tsapis

Impact of polylactide fluorinated-end group length and their dynamics on perfluohexane microcapsules morphology

Guilherme F. Picheth[a,c], Laurence Moine[a*], Sophie Houvenagel[a], Leociley R. A. Menezes[d], Guilherme L. Sassaki[d], Camille Dejean[b], Nicolas Huang[a], Rilton Alves de Freitas[c], Nicolas Tsapis[a*]

[a] Institut Galien Paris-Sud, CNRS, Univ. Paris-Sud, Université Paris-Saclay, 92296 Châtenay-Malabry, France.

[b] BioCIS, CNRS, Univ. Paris-Sud, Université Paris-Saclay, 92296 Châtenay-Malabry, France.

[c] Biopol, Chemistry Department, Federal University of Paraná, 81531-908 Curitiba, PR, Brazil.

[d] NMR Center, Federal University of Paraná, 81531-980. Curitiba, PR, Brazil.

* Corresponding authors at: Institut Galien Paris-Sud, CNRS, Univ. Paris-Sud, Université Paris-Saclay, 92296 Châtenay-Malabry. E-mail address: laurence.moine@u-psud.fr (Laurence Moine), nicolas.tsapis@u-psud.fr (Nicolas Tsapis).

Keywords: Perfluorocarbon microcapsules, perfluorohexane, fluorinated polymers, focused ultrasound, end-group dynamics, fluorous interaction

Table of Content Graphic

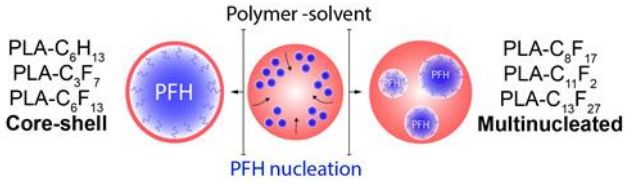

Abstract

We have synthesized polylactide (PLA) polymers containing five distinct lengths of fluorinated end-groups (from C_3F_7 to $C_{13}F_{27}$). The influence of fluorinated end-groups length and their dynamics in chlorinated solvents (chloroform and dichloromethane) was investigated as a function of the presence of perfluohexane (PFH) and related to the morphology of capsules of PFH obtained using these fluorinated polylactides. ^{19}F spin-spin relaxation time (T_2) measurements revealed a reduced mobility of the fluorinated units with dependency on fluorinated chain length in the order C_3F_7>C_8F_{17}>$C_{13}F_{27}$. The presence of perfluorohexane (PFH) led to a further decrease on the segmental mobility, indicating the existence of fluorous interactions. The T_2 relaxation time of the CF_3 resonance of PLA-C_3F_7 decreased from 540±50 ms in $CDCl_3$ to 81±15 ms after the addition of PFH. Due to these fluorous interactions, PLA polymers containing short fluorinated groups (C_3F_7 and C_6F_{13}) led to microcapsules with core-shell morphologies, whereas those formulated with long F-units (C_8F_{17}, $C_{11}F_{23}$ and $C_{13}F_{27}$) favored the formation of multinucleated capsules as observed by confocal microscopy.

1. Introduction

Fully and partly fluorinated compounds are widely explored in the chemical industry and academic research for their inherent immiscibility with hydrophobic and lipophobic solvents. This so-called “fluorophilic” character is responsible for low or “gas like” intermolecular attractions which confer to such molecules inertness and biocompatibility, features that attracted special attention for a wide range of biomedical applications[1,2]. In particular, liquid perfluorocarbons (PFCs), such as perfluorohexane (PFH) or perfluorooctyl bromide (PFOB) are described to be minimally absorbed, eliminated from the lungs by evaporation and did not lead to any significant histological, cellular or biochemical disturbance [3]. Therefore, these PFCs are intensively investigated for their potential to act as intravascular contrast agents [4].

Recent reports describe the use of capsules containing PFOB to provide *in vivo* ^{19}F-MRI or ultrasound detection and also passively deliver chemotherapeutics to cancer cells [5–9]. Similar formulations use PFH as an active core for its lower boiling point, as it favors liquid-to-gas transition by acoustic and thermal stimuli, allowing real-time ultrasonic imaging as well as localized drug-release [10–12]. Nonetheless, the entrapment of fully fluorinated PFCs, such as PFH, within a polymeric shell is proving to be difficult due to their dual lipophobic and hydrophobic character and their trend to easily evaporate during formulation [14]. Several groups have turned to the use of fluorinated surfactants or lipids to improve PFCs encapsulation [15–17]. Literature also reports the functionalization of polymer with fluorinated end-groups to favor interactions with PFCs [11,14,18–24]. It was previously demonstrated that a wide range of fluorinated end-groups linked to the PLA chain – from C_3F_7 to $C_{13}F_{27}$ – increased the entrapment of PFCs into nanocapsules, resulting in more efficient acoustic responses[14,19]. However, no significant distinction regarding the morphology or PFC entrapment was observed by increasing the length of the end-fluorinated groups in nanoformulations.

The main objective of this study is to investigate deeper the influence and extent of fluorous interactions between fluorinated end-groups of PLA-C_xF_{2x+1} and PFH on the final morphology of microcapsules (MC) as a function of fluorinated end-group length. In particular, we examine the role of the solvent in which the polymer was dissolved on the strength of fluorous interactions by comparing chloroform and dichloromethane, two solvents often used to formulate polymer particles and capsules [25,26]. To fully explore the impact of fluorinated end-group chain length and solvent, end-group dynamics and PFH entrapment efficiency were evaluated by NMR and MC morphology was assessed by confocal microscopy. This study provides information for the morphological design of new ultrasound activable systems formulated with fluorinated PLA polymers.

2. Materials and Methods

2.1 Materials

D,L-lactide was purchased from Polysciences (Germany) and perfluorohexane 98+% was acquired from Alfa Aesar (Germany). 1-hexanol was obtained from Acros Organics (Belgium), 2,2,3,3,4,4-heptafluoro-1-butanol, 1H,1H perfluoro-1-heptanol, 1H,1H perfluoro-1-nonanol, 1H,1H perfluoro-1-dodecanol and 1H,1H perfluoro-1-tetradecanol were acquired from Fluorochem (United Kingdom). Acetone, tetrahydrofuran (THF) and dichloromethane were purchased from Carlo Erba Reactifs (France), chloroform and diethyl ether from VWR (France). Nile red, stannous octoate, sodium cholate, trifluoroacetic acid (TFA), deuterated chloroform and deuterated dichloromethane were provided by Sigma-Aldrich (France). The ultrapure water was produced by a RIOS/Milli-Q system (Millipore, France), with a resistivity of 18.2 MΩcm. The NMR sample tubes and coaxial inserts were obtained from CortecNet (France).

2.2 Polymer Synthesis

All fluorinated (PLA-C_3F_7, PLA-C_6F_{13}, PLA-C_8F_{17}, PLA-$C_{11}F_{23}$ and PLA-$C_{13}F_{27}$) and non-fluorinated (PLA-C_6H_{13}) derivatives of polylactide polymers were synthesized by ring opening polymerization (ROP) with the presence of stannous octoate as catalyst [27,28]. All glassware and stir bars were flame-dried and cooled under argon flow. Briefly, in a 10 mL schlenck tube equipped with a magnetic stir-bar, the D,L-lactide (10.4 mmol, 1.5 g) and corresponding initiator (0.075 mmol) – 1-hexanol for PLA-C_6H_{13}, 2,2,3,3,4,4-heptafluoro-1-butanol for PLA-C_3F_7, 1H,1H perfluoro-1-heptanol for PLA-C_6F_{13}, 1H,1H perfluoro-1-nonanol for PLA-C_8F_{17}, 1H,1H perfluoro-1-dodecanol for PLA-$C_{11}F_{23}$ or 1H,1H perfluoro-1-tetradecanol for PLA-$C_{13}F_{27}$ – were added to the flask under argon flow. The tube was sealed with a rubber cap and a stannous octoate solution (0.05 mmol, 20 mg) dissolved in 2 mL of dried toluene was added through the septum. The tube was purged with argon for 0.5 h and the polymerization reaction was conducted with continuous stirring at 130 °C for 55 minutes in an oil bath under

argon flow. The reaction was quenched by immersing the flask in a cold water bath. Afterwards, the solvent was evaporated under reduced pressure for 1h and the material was dissolved in 5 mL of chloroform. The product was purified by precipitation as previously described[29]: all polymers were precipitated into cold diethyl ether (80 mL), next, PLA-C_6H_{13} was dissolved into THF (5 mL), whereas the fluorinated polymers were dissolved in acetone (20 mL) and precipitated again in ultrapure water (150 mL). The samples were freeze-dried for 24 h and a white powder was obtained. Lactide conversion ≥95% (^{1}H-NMR). ^{1}H-NMR [400 MHz, $CDCl_3$, 25°C] **PLA-C_6H_{13}**: δ_H 5.10-5.28 (PLA-C*H*CH_3COO-), 1.52-1.61 (PLA-CHC*H*$_3$COO-), 0.88-0.92 (-CH_2C*H*$_3$). **PLA-C_3F_7, PLA-C_6F_{13}, PLA-C_8F_{17}, PLA-$C_{11}F_{23}$ and PLA-$C_{13}F_{27}$**: δ_H 5.10-5.28 (PLA-C*H*CH_3COO-), 4.50-4.70 (-OC*H*$_2$$CF_2$-), 1.52-1.61 (PLA-CHC*H*$_3$COO-). ^{19}F-NMR [400 MHz, $CDCl_3$, 25°C] **PLA-C_3F_7**: δ_F -79.0 (-C*F*$_3$), -118.7 (-OCH$_2$C*F*$_2$-) and -125.7 (-C*F*$_2$$CF_3$); **PLA-$C_6F_{13}$, PLA-$C_8F_{17}$, PLA-$C_{11}F_{23}$ and PLA-$C_{13}F_{27}$:** δ_F -78.9 (-C*F*$_3$), -117.7 (-OCH$_2$C*F*$_2$-), -120.0 (-(C*F*$_2$)$_n$$CF_2CF_3$), -120.7 (-OCH$_2$$CF_2CF_2$C*F*$_2$-), -121.4 (-OCH$_2$$CF_2$C*F*$_2$-) and -124.2 (-C*F*$_2$$CF_3$).

2.3 Characterization

All polymers were characterized by size exclusion chromatography (SEC) in chloroform at 30 °C with a flow rate of 1 mL.min^{-1} by two columns (PL-gel 5µm MIXED-D 300 x 7.5 mm) calibrated against a curve based on poly(methyl methracrylate) standards (PMMA, Polymer Laboratories, Varian Inc.) The system was coupled to a refractive index detector (Spectrasystem RI-150, Thermo Electro Corp.). ^{1}H and ^{19}F-NMR spectra were obtained on a Bruker AVANCE III HD 400 MHz in $CDCl_3$ at 25ºC.

2.4 Interfacial surface tension

The interfacial surface tension was performed in a Tracker tensiometer (Teclis, France). PFH was previously filtrated by a column of aluminum oxide. A constant 2 µL PFH or sodium cholate drop was formed by a syringe and a G20 stainless steel needle inside an optical glass cuvette containing fixed polymer concentrations of 25 mg.mL^{-1} in chloroform or

dichloromethane previously filtered by 0.22 µm (Millipore). The temperature was kept at 20 °C and the interfacial surface tension was determined from the drop profile employing the Laplace equation and the forces balance between capillarity and gravity.

2.5 ^{19}F-NMR T_1 and T_2 Relaxation

^{19}F Spin-lattice and spin-spin relaxation measurements were performed at 25 ºC in $CDCl_3$ or CD_2Cl_2 with fixed polymer concentrations of 25 mg.mL^{-1}. Samples containing 15 µL of PFH were also evaluated. The samples were not degassed. All experiments were performed on a Bruker AVANCE III HD NMR spectrometer operating at 9.4 T, equipped with a 5-mm multinuclear inverse detection probe, observing ^{19}F and ^{1}H nuclei at 376.49 and 400.13 MHz, respectively. ^{19}F T_1 was determined by the inversion-recovery pulse sequence (T_1IR). The delay (τ) between the inversion and read-pulse was varied along 16 values (1 to 22 s). The total number of scans was 32, spectral width = 100 ppm and relaxation delay = 22 s. ^{19}F T_2 values were measured by the PROJECT-CPMG pulse sequence along 15 values of τ (0.1 to 2 ms) [30]. The number of scans was 128, spectral width = 100 ppm and relaxation delay = 10 s. Relaxation times were obtained by nonlinear least-squares fitting of a mono- exponential function with $r^2 \geq 0.998$ for all samples.

2.6 Microcapsules Formulation

Microcapsules were prepared by the emulsion-evaporation technique, as previously described [13], with minor modifications. Briefly, the desired amount of polymer was dissolved into 2 mL of chloroform or dichloromethane in a 50 mL glass flask. Afterwards, 50 µL of nile red (55 µg.mL^{-1}) was added and the flask was sealed with a rubber cap. Next, 30 µL of PFH was introduced through the septum with constant stirring and the media was emulsified with 10 mL of sodium cholate 1.5% (w/w) at 4 °C. The mixture was submitted to high-speed homogenization at 8.000 RPM using an Ultra-Turrax T25 (IKA) coupled with an SN25-10G dispersing tool in an ice bath for 1 minute. The solvent was removed by rotary evaporation

(Büchi) with a 30 °C water bath and recirculation chiller at -10 °C. A vacuum gradient from 400 to 30 mbar in 7 steps of 5 minutes was employed. Afterwards, the total volume of each sample was completed to 10 mL with ultrapure water.

2.7 Confocal Microscopy

Microcapsules were washed twice with ultrapure water by centrifugation and resuspended in glycerol to minimize motion. All samples were observed in a Leica TCS SP5 confocal scanning microscope (Leica) with a 1 mW helium neon laser operating at excitation of 551 nm and 636 nm of emission, Plan Achromat 63X objective (NA 1.40 oil immersion) and pinhole diameter at 71 nm. For diameter analysis, the measurements were performed in the equatorial plane of each capsule as previously described [13].

2.8 Scanning Electron Microscopy

Scanning electron microscopy was performed in a Merlin 6040 (Carl Zeiss, Germany) operating at 3 kV. All microcapsules were washed twice with ultrapure water by centrifugation to remove the excess of sodium cholate, deposited on carbon conductive double-sided tape (Euro-medex, France) and dried at room temperature. Afterwards, they were coated with a palladium–platinum layer of about 3 nm using a Cressington sputter-coater 208HR with a rotary-planetary-tilt stage, fitted with an MTM-20 thickness controller.

2.9 PFH encapsulation efficiency by ^{19}F-NMR spectroscopy

For PFH quantification, 1 mL of microcapsules was freeze-dried during 24 h employing an Alpha-1-2 LD apparatus (Christ). The flasks were hermetically sealed with a rubber cap and stored at -20 °C until analysis. The PFH encapsulation efficiency was determined as described by Diou *et al.* [29]. A total volume of 1 mL of chloroform was introduced into the sealed tube by a needle, the suspension was vortexed (5 cycles of 30 seconds) and centrifuged at 0 °C for 10 minutes at 5000 rpm (Jouan CR4I centrifuge, Thermo Electron Corporation). The organic solution was collected in a cold room at 4 °C and introduced into

an NMR tube that was afterwards loaded with a stem coaxial insert containing TFA in D_2O (12 µmol.mL^{-1}) as external standard [31]. All spectra were obtained at 4 °C on a Bruker Avance 300 (400 MHz) spectrometer. The total amount of encapsulated PFH was determined based on a PFH calibration curve. For each MC sample, the integration of the TFA peak at -76.5 ppm was determined as 3 and the resulting integration of the PFH CF_3 at -81.2 ppm was used to calculate the PFH concentration in the NMR tube based to the equation of the calibration curve.

2.10 Statistical analysis

The statistical analysis was performed using Statistica™ 8.0 software (StatSoft Inc., Tulsa, USA). The data was analyzed by two-sided Student's *t*-test and a statistical significance was set at the level of $p<0.05$.

3. Results and Discussion

3.1 Polymers synthesis and characterization

Six end-group fluorinated or alkylated polymers were synthesized by ring opening polymerization of D,L-lactide with appropriate initiator (hexanol or fluorinated alcohols) as previously described [14,19,28,32] (reaction yield > 85%). The polylactide main chain is constituted by ~140 repetitive units containing different lengths of end fluorinated-groups: polymers are designated according to the terminal group chemistry and length of fluorinated units as PLA-C_6H_{13}, PLA-C_3F_7, PLA-C_6F_{13}, PLA-C_8F_{17}, PLA-$C_{11}F_{23}$ and PLA-$C_{13}F_{27}$. They were characterized by ^{1}H and ^{19}F-NMR and exhibited a molecular weight around 18000-21000 g.mol^{-1} as assessed by NMR, with a narrow dispersity (Supporting information **Figure S1 and Table S1**).

3.2 Polymers dynamics

To explore the role and extent of fluorous interactions between the different PLA-C_xF_{2x+1} and PFH during the formation of microcapsules, we have investigated interfacial properties, dynamics in solution as well as morphological features generated by each of these polymers. As fluorine recognition and compartmentalization are strictly dependent on the solvent's character, the behavior and impact of polymer end-group chemistry was studied in two distinct solvents usually employed in the formulation of MC, namely, chloroform and dichloromethane[25,26].

The interfacial activity of the polymers was determined at the solvent/PFH and solvent/sodium cholate (SC) interfaces by interfacial surface tension measurements (**Table 1**). At the solvent/SC interface, interfacial tension values were between 7–8 mN.m^{-1} in $CHCl_3$ or CH_2Cl_2, for all polymers, suggesting no specific solvent or end-group contribution to the interfacial activity. At the PFH/solvent interface, polymers dissolved in $CHCl_3$ exhibited an interfacial tension average value of 3.0±0.05 mN.m^{-1} whereas 6.0±0.1 mN.m^{-1} was measured for polymers dissolved in CH_2Cl_2, indicating that $CHCl_3$ favors PFH spreading. Nonetheless,

198 none of the polymers was able to decrease the interfacial tension compared to the solvent
199 itself regardless the end-group chemistry or the length of the fluorinated end-group.

200 **Table 1**. Interfacial tensions at the perfluorohexane/solvent and alkylated or fluorinated
201 polymer/sodium cholate 1.5% (w/v) interfaces. All polymers were dissolved at 25 mg.mL^{-1} in
202 chloroform or dichloromethane. All results are expressed in mN.m^{-1}.

	Chloroform		**Dichloromethane**	
	PFH/solvent	**Solvent/SC 1.5%**	**PFH/solvent**	**Solvent/SC 1.5%**
Solvent	3.2±0.3	7.5±0.3	6.0±0.3	8.1±0.2
PLA-C_6H_{13}	3.0±0.5	7.5±0.2	6.2±0.5	8.0±0.2
PLA-C_3F_7	3.0±0.3	7.0±0.1	6.1±0.7	7.5±0.3
PLA-C_6F_{13}	3.0±0.5	7.1±0.5	6.2±0.4	7.7±0.5
PLA-C_8F_{17}	3.1±0.4	7.1±0.2	5.9±0.4	7.7±0.4
PLA-$C_{11}F_{23}$	3.0±0.3	7.2±0.3	5.9±0.3	7.8±0.2
PLA-$C_{13}F_{27}$	3.1±0.4	7.4±0.1	6.1±0.4	7.6±0.1

203 PFH-SC (1.5% w/v) interfacial tension was 22.5±0.2 mN.m^{-1}

204 The lack of adsorption at the PFH/solvent interface might be explained by the mass ratio
205 difference between the relatively small fluorinated blocks compared to the PLA main chain
206 (C_3 to C_{13} for fluorinated block vs. 140 repetitive units for PLA) and the conformation
207 assumed by the polymer in solution. Indeed, as the PLA polymers are well solvated in $CHCl_3$
208 and CH_2Cl_2 (Hildebrand solubility parameter (δ_T) of 20.8 MPa$^{0.5}$ for unmodified PLA, 18.7
209 MPa$^{0.5}$ for $CHCl_3$ and 20.2 MPa$^{0.5}$ for CH_2Cl_2 [33]), a conformational rearrangement based on
210 the higher solubility of the polymeric chains within the solvents may hide the fluorinated
211 groups inside the PLA coil, hindering an effective interaction with the PFH phase [19].

212 Although no interfacial activity was observed at the PFH/solvent interface during static
213 measurements, the solvent-evaporation process is dynamic and associated with transitory
214 interfacial instabilities due to system disorganization [34]. Such constant rearrangement of
215 water and organic solvent molecules may promote the formation of fluorinated domains

favorable for PFH encapsulation [35]. Indeed, many studies carried on mixed systems, containing both fluorocarbons and organic solvents, showed the tendency of perfluoralkyl moieties to self-associate and generate fluorous compartments. This aggregation in rich fluorous domains is generally associated to a reduced mobility of fluorinated groups [26,36,37].

To assess the behavior of the fluorinated chains in a more dynamic media containing PFH – a situation similar to what happens prior to solvent evaporation – the end-group mobility of three fluorinated polymers, PLA-C_3F_7, PLA-C_8F_{17} and PLA-$C_{13}F_{27}$, was analyzed by fluorine NMR spectroscopy employing spin-lattice (T_1) and spin-spin (T_2) relaxation measurements at fixed polymer concentration of 25 $mg.mL^{-1}$ and 15 µL of PFH (corresponding to the formulation conditions). Accordingly, the CF_3 group dynamics in each solvent was probed in presence and absence of PFH in the solvent. Unfortunately, some of the PFH resonances overlapped with the CF_3 polymer signals for PLA-C_8F_{17} and PLA-$C_{13}F_{27}$ in both solvents. Only PLA-C_3F_7 exhibited well segregated resonance from those of PFH because of the different chemical environments, which permitted a resonance shift towards lower magnetic fields, not overlapping with PFH as displayed in **Figure 1.** The nomenclature and ^{19}F-NMR peak labeling consists alphabetically with the position of the fluorinated resonance respective to the PLA chain [38,39].

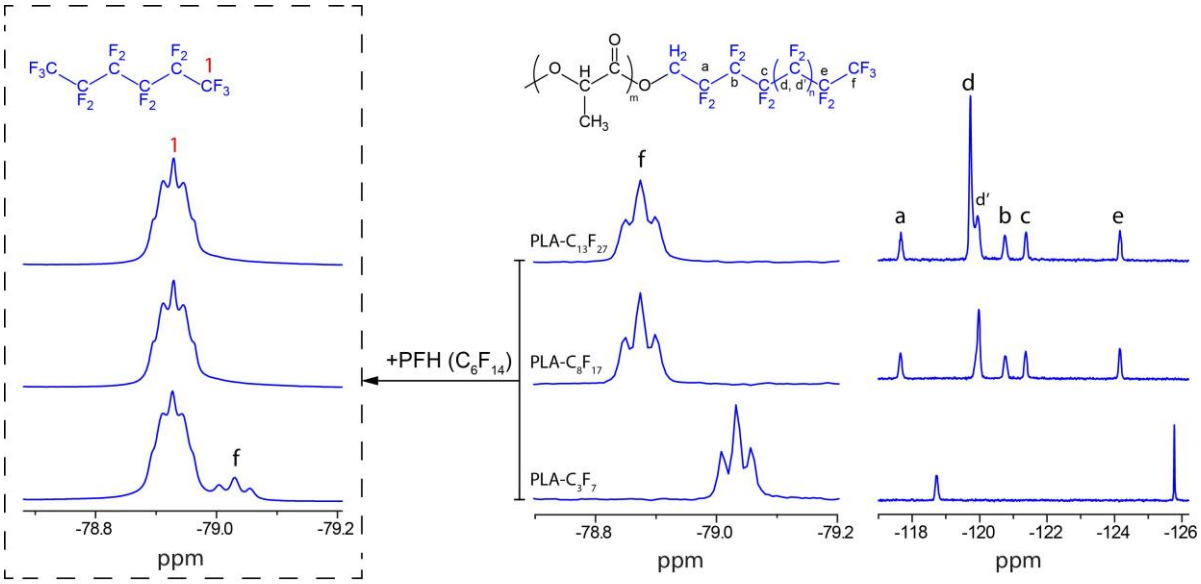

234

235 **Figure 1**. Magnified CF_3 and CF_2 regions of the ^{19}F-NMR spectra for PLA-C_3F_7, PLA-C_8F_{17}
236 and PLA-$C_{13}F_{27}$ in $CDCl_3$. The insets (left) exhibit the CF_3 resonance in a mixed system of
237 polymer and perfluorohexane. ^{19}F peak assignment is indicated in the top of each image.

238 T_2 analysis revealed that the CF_3 resonance mobility decreased strongly for polymers
239 functionalized with longer fluorinated units in the order C_3F_7>C_8F_{17}>$C_{13}F_{27}$ for both solvents
240 (**Table 2**). Such reduction in the local fluorine dynamics according to chain length is related
241 to the strong electronegativity of the C-F bond that generates linear and rigid chain
242 conformations, reducing the segmental mobility as the chain length increases [40].
243 Nonetheless, samples dissolved in $CDCl_3$ showed smaller relaxation values compared to
244 their counterparts prepared in CD_2Cl_2: this effect is clearly illustrated by the CF_3 resonance of
245 PLA-C_3F_7, with T_2 of 540±50 ms in $CDCl_3$ and 1530±150 ms in CD_2Cl_2. Such results were also
246 confirmed by T_1 measurements (Supporting information **Table S2**). These significant
247 changes in relaxation times indicate that chloroform is not a good solvent for the fluorinated
248 end-groups and drives self-association of ^{19}F containing units.

249

Table 2. ^{19}F spin-spin relaxation (T_2) values of CF_3 resonances for samples dissolved in deuterated chloroform or dichloromethane in presence of absence of perfluorohexane. All polymers were dissolved at fixed concentration of 25 $mg.mL^{-1}$ (Experiment performed in duplicate, n=2).

Sample	**T_2 (ms)**		**T_2 (ms)**	
	$CDCl_3$	**$CDCl_3$+PFH**	**CD_2Cl_2**	**CD_2Cl_2+PFH**
PLA-C_3F_7	540±50	81±15	1530±150	1710±250
PLA-C_8F_{17}	210±20	---	1263±165	---
PLA-$C_{13}F_{27}$	76±10	---	790±50	---

Afterwards, PFH was added to each polymer solution to simulate the system behavior just before emulsification with sodium cholate. In CD_2Cl_2, T_2 varied from 1530±150 ms to 1710±250 ms in presence of PFH, showing that the end-group dynamics is not significantly affected by PFH addition in the media ($p = 0.475$). However, in $CDCl_3$, the CF_3 signal of PLA-C_3F_7 showed a significant T_2 decrease with PFH, from 540±50 ms to 81±15 ms ($p < 0.05$). This lower mobility denotes a polymer rearrangement in presence of PFH evidencing an increased tendency for the fluorinated segments to associate with each other (**Figure 2**). Indeed, in $CHCl_3$, addition of PFH further decreases the solubility of the fluorinated segments which promotes dipolar interactions between the fluorinated end-group and PFH. These more efficient interactions in $CHCl_3$ suggest formation of F-rich domains where the reduced mobility of the fluorinated segment leads to shorter T_2 values.

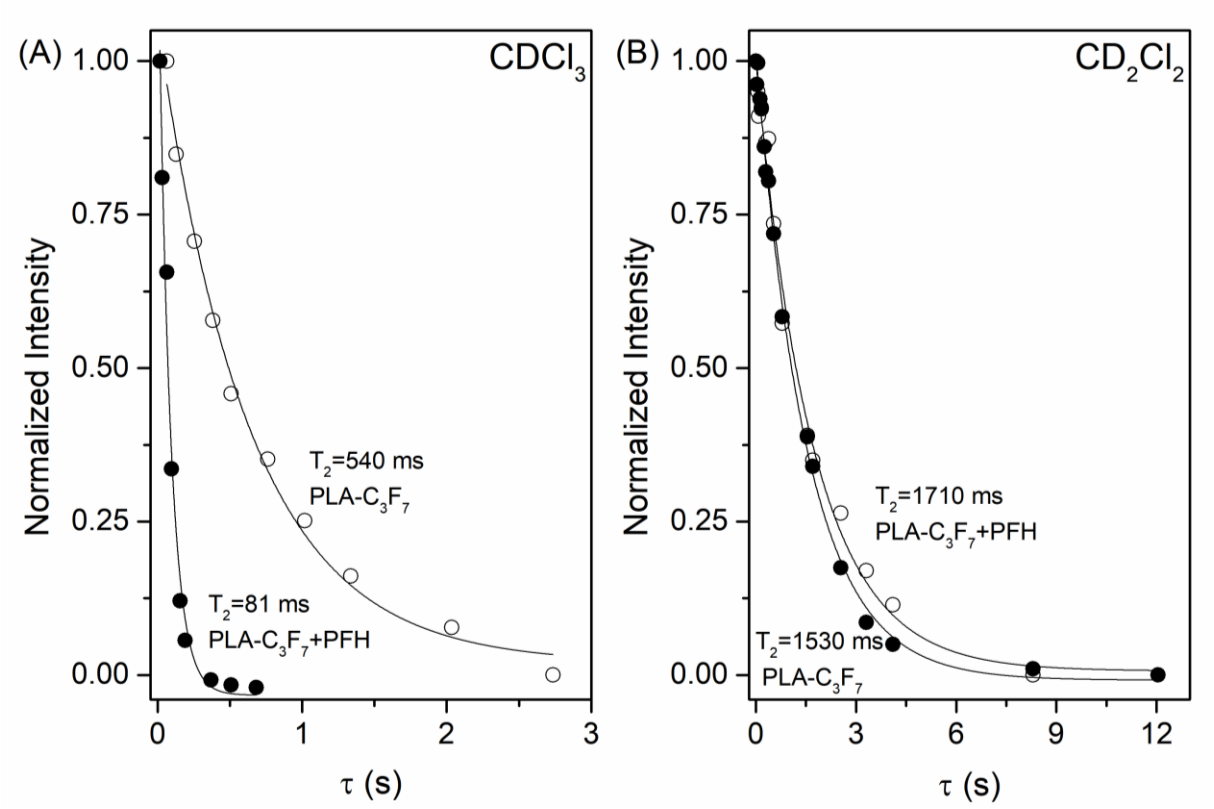

Figure 2. T_2 decay profiles for the CF_3 resonance of PLA-C_3F_7 in $CDCl_3$ (A) and CD_2Cl_2 (B) without (open circles) and with perfluorohexane (dark circles).

According to those results, the introduction of PFH was able to reduce the local end-fluorinated group mobility of PLA-C_3F_7 in $CDCl_3$. As PFH is well dissolved in chloroform, its contact with the fluorinated units may lead to the formation of fluorophilic domains, a process that might also depends on the length of the fluorinated group. This scenario, however, illustrates the system's behavior only in stable organic solutions; during the solvent-evaporation process in which MCs are formulated, transitory and thermodynamically unstable interfaces are created. Therefore, the ability of each fluorinated derivative to better stabilize and retain PFH as a liquid core was further studied in MCs formulations.

3.2 Solvent Influence on MC formulation

The impact of the fluorinated end-groups on the final morphology of microcapsules was then studied for all synthesized polymers. All microcapsules were initially formulated with fixed amounts of polymer (50 mg) that were dissolved either in chloroform or dichloromethane and

subsequently submitted to the same solvent-evaporation process. The encapsulation efficiency (EE) of PFH was quantified in freeze-dried samples by ^{19}F-NMR and the size of all MCs was measured by confocal microscopy as listed in **Table 3**.

Table 3. Encapsulation efficiency and size of microcapsules formulated with 50 mg of polymer prepared in chloroform and dichloromethane.

Sample	**Chloroform**		**Dichloromethane**	
	Size (µm)*****	PFH EE (%)	Size (µm)*****	PFH EE (%)
PLA-C_6H_{13}	4.2±1.0	5.5±0.2	4.8±0.8	12.3±0.2
PLA-C_3F_7	4.4±0.6	10.1±0.2	4.7±0.8	9.1±0.1
PLA-C_6F_{13}	4.8±1.0	12.7±0.2	4.6±1.0	13.1±1.3
PLA-C_8F_{17}	4.6±0.8	10.3±0.5	4.9±1.2	11.1±0.2
PLA-$C_{11}F_{23}$	5.2±1.4	11.1±1.4	4.8±0.9	7.1±0.1
PLA-$C_{13}F_{27}$	5.2±1.0	11.4±1.5	5.3±0.6	10.0±0.7

*****All measurements correspond to observation and analysis of at least 100 microcapsules per each group.

As determined by ^{19}F NMR, the non-fluorinated polymer, PLA-C_6H_{13}, presented an encapsulation efficiency of 5.5±0.1% when prepared in $CHCl_3$. The use of fluorinated polymers led to a 2-fold increase in PFH encapsulation efficiency, reaching 11±3.0% without any significant distinction as a function of the fluorinated end-group length (**Table 3**). The reduced end-group mobility of fluorinated polymers in $CDCl_3$ containing PFH was translated into higher encapsulation efficiencies. Altogether, these results evidence the ability of fluorinated polymers to interact with the fluorocarbon phase and enhance its stabilization inside the organic phase, as previously reported for nanocapsules [14]. For microcapsules prepared in CH_2Cl_2, no trend was observed for the encapsulation efficiency, probably due the absence of specific interactions between PFH and the polymer (Table 2).

Nonetheless, PLA or PLGA polymers are able to encapsulate higher amounts of PFH into MCs (~40%) [13], the discrepancy with our results may be related to the fast process of solvent

evaporation employed here, whereas Mousnier et al. have evaporated the organic solvent slowly at ambient pressure[13].

Although all samples were predominately smooth as shown by SEM in **Figures 3 and 4 (bottom)**, a certain amount of rough shelled MCs were also observed in all images. According to Chung, *et al.*, this morphological variation might be related to the fast evaporation process used, which promoted an uneven polymer concentration gradient towards the interface [41]. Also, a partial PFH vaporization during the solvent evaporation step (performed at 30 °C) may have caused a volumetric expansion of the MCs and, as the temperature dropped, a subsequent shrinkage altered the continuous spreading of the polymer at the interface as previously reported by Lebeveda *et al.* for PFH containing microspheres [42].

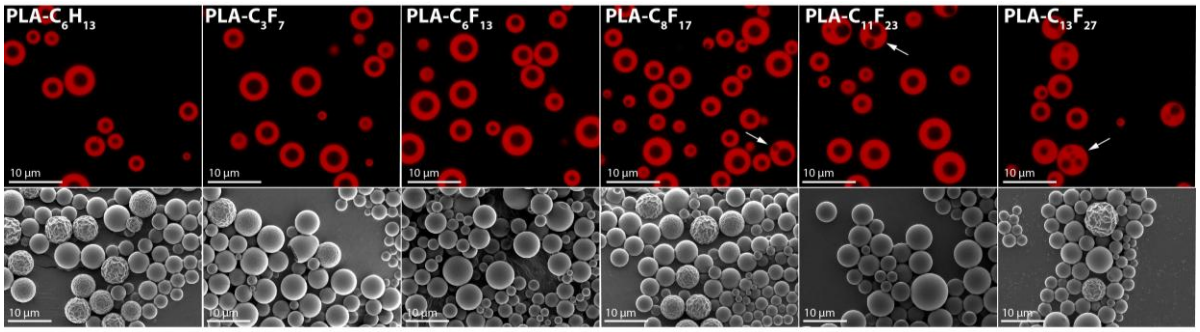

Figure 3. Confocal (top) and scanning electron microscopy (bottom) images of microcapsules produced in chloroform. Scale bar represents 10 µm.

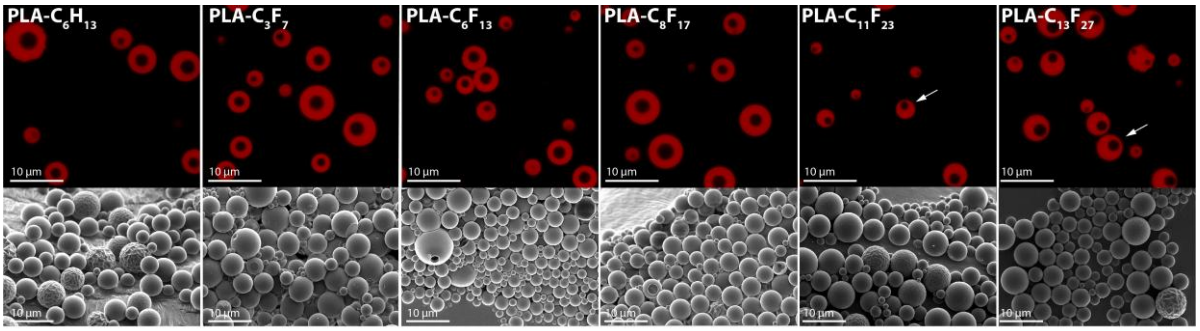

Figure 4. Confocal (top) and scanning electron microscopy (bottom) images of microcapsules produced in dichloromethane. Scale bar represents 10 µm.

A clear and subtle distinction on MC morphology was observed according to the fluorinated end-group length in both solvents. In all cases, PLA-C_6H_{13}, PLA-C_3F_7 and PLA-C_6F_{13} exhibited core-shell morphologies comprising a well-centered PFH phase; however, as the end-group length increased to C_8F_{17}, $C_{11}F_{23}$ and $C_{13}F_{27}$ higher extents of randomly distributed PFH cores were observed as displayed by the white arrows in **Figures 3 and 4 (top)**. In CH_2Cl_2, MCs still possess a distinctive core shell structure but the inner PFH core is displaced from the center of the MC. Such decentered morphology had already been observed [13]. Formulation in $CHCl_3$ leads to a mixture of structure with well centered MC and with MC having multi-cores of PFH.

Regardless of the solvent employed, samples prepared with short fluorinated or non-fluorinated end-groups, PLA-C_3F_7 and PLA-C_6F_{13} or PLA-C_6H_{13}, presented the formation of core-shell capsules. Only MCs formulated with longer fluorinated groups, PLA-C_8F_{17}, PLA-$C_{11}F_{23}$ and PLA-$C_{13}F_{27}$, led to the appearance of different morphologies, either in chloroform or dichloromethane, indicating that the shell precipitates prior to complete PFH nucleation at the center of the organic droplet. Thus, the length of the fluorinated end-group played an important role in the fluorocarbon nucleation process, suggesting that longer fluorous chains were able to better interact and restrain the PFH diffusion as illustrated in **Figure 5**.

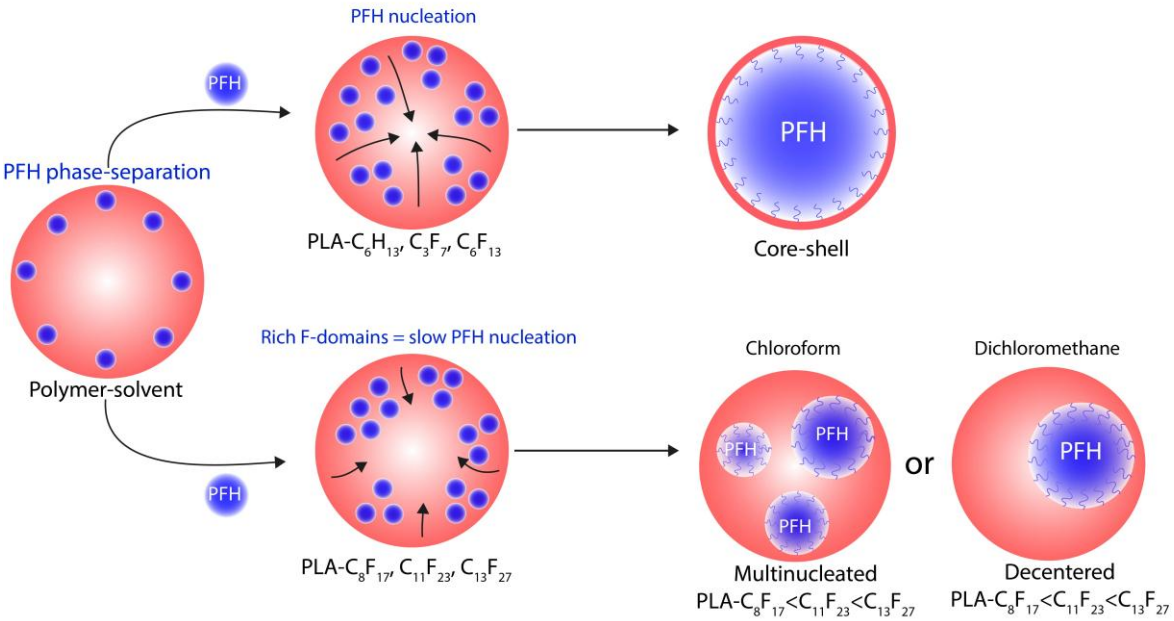

Figure 5. Schematic representation of the perfluorohexane phase-separation and nucleation process in the organic phase containing fluorinated polymers of distinct end-group lengths.

The different morphologies generated in each solvent are possibly related with the extent of fluorous interactions, PFH miscibility as well as solvent evaporation rate. In dichloromethane, the formation of decentered capsules for the longer F-units samples, such as PLA-$C_{13}F_{27}$, probably reflected the reduced extent of interactions between the end-groups and PFH. Nonetheless, such samples were still able to alter the nucleation pattern, inducing the PFH to accumulate towards the drop's periphery, also suggesting the fluorinated segregation effect. The obtained decentered morphologies are, however, favored by the solvent's lower boiling point (39.6 °C for CH_2Cl_2 vs. 61.2 °C for $CHCl_3$) that accelerates the onset of polymer precipitation.

In chloroform, the shell of polymers with longer fluorinated groups precipitates before the complete fluorocarbon nucleation restraining PFH diffusion and causes multiple PFH cores dispersed inside the rigid polymeric phase. As disclosed by T_2 results, the PFH is able to interact more efficiently with the fluorinated end-groups in this solvent. Thus, such structure

352 is probably attributable to formation of F-rich domains driven by the end-group polymer
353 arrangement to minimize contact with the surrounding polymer. This effect indicates that
354 longer fluorinated units interact more importantly with PFH.

355 ***3.3 Influence of polymer concentration on MC morphology***

356 To further evaluate the end-group chemistry and length influence on microcapsules structure,
357 samples PLA-C_6H_{13}, PLA-C_3F_7, PLA-C_8F_{17} and PLA-$C_{13}F_{27}$ were prepared only in chloroform
358 using different polymer masses (12.5, 25, 50 and 100 mg) and constant PFH volume of 30
359 µL.

360 Samples prepared with 12.5 mg presented core-shell structures with thin and smooth
361 polymer layers that were predominant for all polymers, independently of end-group chemistry
362 or length as shown in **Figure 6**. The increase of polymer mass to 25 mg altered only the
363 morphology of MCs having the longest fluorinated group: PLA-$C_{13}F_{27}$ by formation of
364 multinucleated capsules (42±10%) as displayed by the white arrow in **Figure 6**. The
365 percentage of multiple PFH cores for PLA-$C_{13}F_{27}$ became more obvious for 50 and 100 mg,
366 in which the total amount of multinucleated MCs increased from 60±5% to 91±3%,
367 respectively. The same effect but at a lower extent was observed for PLA-C_8F_{17}, as thin-
368 shelled MCs are observed in the formulations containing 25 mg and multinucleated
369 morphologies increased from 10±2% to 56±7% for 50 and 100 mg, respectively. A similar
370 behavior was observed for MC formulated with the polymer containing the shortest fluorine
371 end-group, PLA-C_3F_7, as core-shell structures predominated until a polymer mass of 100 mg,
372 in which a total of 45±5% of multinucleated MC were found. In contrast, MC formulated with
373 the non-fluorinated sample, PLA-C_6H_{13}, exhibited core-shell morphologies for all of the tested
374 polymer masses.

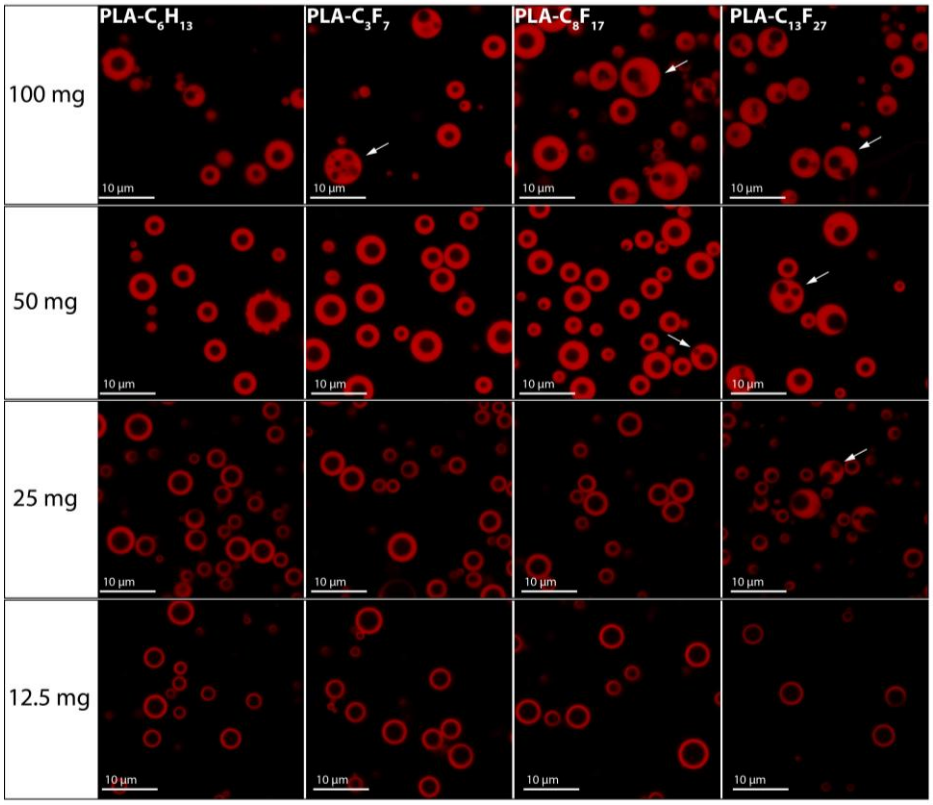

Figure 6. Confocal microscopy images of microcapsules formulated in chloroform with non-fluorinated (PLA-C_6H_{13}) and fluorinated (PLA-C_3F_7, PLA-C_8F_{17} and PLA-$C_{13}F_{27}$) polymers with varied polymer masses: 100, 50, 25 and 12.5 mg. Scale bar of 10 µm.

Despite heterogeneity of morphology within the same sample, a clear effect of the polymer end-group chemistry and fluorinated length was evidenced in the capsule's morphology. Compared to PLA-C_6H_{13}, polymers containing F-groups generated MCs with decentered and/or multiple PFH cores. At high fluorinated polymer mass, the dominant morphology whatever the fluorinated length block consists in multinucleated capsules. This increase in polymer mass favored the formation of richer fluorophilic domains – in the order of C_3F_7<C_8F_{17}<$C_{13}F_{27}$ – that altered the polymeric phase dynamics, reducing the migration of PFH to the center of the organic drop.

4. Conclusion

We have successfully synthesized and characterized poly(lactide) end-group fluorinated polymers for improved fluorous interaction with PFH. The presence of fluorinated end-groups

provided more favorable interfaces with perfluorohexane in organic solution of chloroform with fluorinated end-group length dependency, as revealed by spin-spin relaxation measurements. The formation of fluorophilic environment is reflected with improved perfluorohexane encapsulation efficiencies into microcapsules and by modifying the final morphology, particularly in the case of longer fluorinated end-groups and important polymer masses.

5. Acknowledgements

This work has been supported by the Région Ile-de-France in the framework of DIM Nano-K and the French National Research Agency (ANR) under grant ANR-10-NANO-06 as part of the "Investissements d'Avenir" program. Institut Galien Paris-Sud is a member of the Laboratory of Excellence LERMIT supported by a grant from ANR (ANR-10-LABX-33). We are also thankful to Conselho Nacional de Desenvolvimento Científico e Tecnológico (CNPq) for the financial support, to Valerie Nicolas from MIPSIT for helping with confocal experiments, to Prof. Jaísa Soares as well as Prof. Jens Dittmer for their help with NMR relaxation experiments and to Carine Van-Heijenoort, Christina Sizun and Marc-André Delsuc for fruitful discussions.

Supporting Information.

^{1}H and ^{19}F-NMR spectra of all synthesized polymers in CDCl3.

SEC chromatogram of all polymers in chloroform at 30°C.

Number-average molar masses (Mn) obtained by SEC/1H-NMR, dispersity and glass-transition temperature (Tg) of all polymers.

Spin-lattice relaxation (T1) values of correspondent ^{19}F resonances for samples dissolved in CDCl3 and CD2Cl2 with and without perfluorohexane.

References

(1) Krafft, M. P.; Riess, J. G. Perfluorocarbons: Life Sciences and Biomedical Uses - Dedicated to the Memory of Professor Guy Ourisson, a True RENAISSANCE Man. *J. Polym. Sci. Part a-Polymer Chem.* **2007**, *45* (7), 1185–1198. https://doi.org/10.1002/pola.21937.

(2) Krafft, M. P.; Riess, J. G. Chemistry, Physical Chemistry, and Uses of Molecular Fluorocarbon-Hydrocarbon Diblocks, Triblocks, and Related Compounds-Unique "Apblar" Components for Self-Assembled Colloid and Interface Engineering. *Chem. Rev.* **2009**, *109* (5), 1714–1792. https://doi.org/10.1021/cr800260k.

(3) Shaffer, T. H.; Foust, R.; Wolfson, M. R.; Miller, T. F. Analysis of Perfluorochemical Elimination from the Respiratory System. *J. Appl. Physiol.* **1997**, *83* (3), 1033–1033. https://doi.org/10.1152/jappl.1997.83.3.1033.

(4) Cosco, D.; Fattal, E.; Fresta, M.; Tsapis, N. Perfluorocarbon-Loaded Micro and Nanosystems for Medical Imaging: A State of the Art. *J. Fluor. Chem.* **2015**, *171*. https://doi.org/10.1016/j.jfluchem.2014.10.013.

(5) Pisani, E.; Tsapis, N.; Galaz, B.; Santin, M.; Berti, R.; Taulier, N.; Kurtisovski, E.; Lucidarme, O.; Ourevitch, M.; Doan, B. T.; et al. Perfluorooctyl Bromide Polymeric Capsules as Dual Contrast Agents for Ultrasonography and Magnetic Resonance Imaging. *Adv. Funct. Mater.* **2008**, *18* (19). https://doi.org/10.1002/adfm.200800454.

(6) Jafari, S.; Diou, O.; Mamou, J.; Renault, G.; Fattal, E.; Tsapis, N.; Bridal Lori, S. High-Frequency (20 to 40 MHz) Acoustic Response of Liquid-Filled Nanocapsules. *IEEE Trans. Ultrason. Ferroelectr. Freq. Control* **2014**, *61* (1). https://doi.org/10.1109/TUFFC.2014.6689771.

(7) Diou, O.; Tsapis, N.; Giraudeau, C.; Valette, J.; Gueutin, C.; Bourasset, F.; Zanna, S.; Vauthier, C.; Fattal, E. Long-Circulating Perfluorooctyl Bromide Nanocapsules for Tumor Imaging by (FMRI)-F-19. *Biomaterials* **2012**, *33* (22), 5593–5602. https://doi.org/10.1016/j.biomaterials.2012.04.037.

(8) Boissenot, T.; Fattal, E.; Bordat, A.; Houvenagel, S.; Valette, J.; Chacun, H.; Gueutin, C.; Tsapis, N. Paclitaxel-Loaded PEGylated Nanocapsules of Perfluorooctyl Bromide as Theranostic Agents. *Eur. J. Pharm. Biopharm.* **2016**, *108*, 136–144. https://doi.org/10.1016/j.ejpb.2016.08.017.

(9) Boissenot, T.; Bordat, A.; Larrat, B.; Varna, M.; Chacun, H.; Paci, A.; Poinsignon, V.; Fattal, E.; Tsapis, N. Ultrasound-Induced Mild Hyperthermia Improves the Anticancer Efficacy of Both Taxol® and Paclitaxel-Loaded Nanocapsules. *J. Control. Release* **2017**, *264*. https://doi.org/10.1016/j.jconrel.2017.08.041.

(10) Singh, R.; Husseini, G. A.; Pitt, W. G. Phase Transitions of Nanoemulsions Using Ultrasound: Experimental Observations. *Ultrason. Sonochem.* **2012**, *19* (5), 1120–1125. https://doi.org/10.1016/J.ULTSONCH.2012.02.005.

(11) Li, H.; Wang, J.; Wang, P.; Zheng, J.; Song, F.; Yin, T.; Zhou, G.; Zheng, R.; Zhang, C. Phase-Transition Contrast Nanocapsules Triggered by Low-Intensity Ultrasound. *Chem. Commun.* **2014**, *50* (96), 15163–15166. https://doi.org/10.1039/C4CC04641B.

(12) You, Y.; Wang, Z.; Ran, H.; Zheng, Y.; Wang, D.; Xu, J.; Wang, Z.; Chen, Y.; Li, P. Nanoparticle-Enhanced Synergistic HIFU Ablation and Transarterial Chemoembolization for Efficient Cancer Therapy. *Nanoscale* **2016**, *8* (7), 4324–4339. https://doi.org/10.1039/C5NR08292G.

(13) Mousnier, L.; Huang, N.; Morvan, E.; Fattal, E.; Tsapis, N. Influence of Polymer End-Chemistry on the Morphology of Perfluorohexane Polymeric Microcapsules Intended as Ultrasound Contrast Agents. *Int. J. Pharm.* **2014**, *471* (1–2). https://doi.org/10.1016/j.ijpharm.2014.05.012.

(14) Picheth, G.; Houvenagel, S.; Dejean, C.; Couture, O.; Alves de Freitas, R.; Moine, L.; Tsapis, N. Echogenicity Enhancement by End-Fluorinated Polylactide

Perfluorohexane Nanocapsules: Towards Ultrasound-Activable Nanosystems. *Acta Biomater.* **2017**, *64*. https://doi.org/10.1016/j.actbio.2017.10.002.

(15) Astafyeva, K.; Somaglino, L.; Desgranges, S.; Berti, R.; Patinote, C.; Langevin, D.; Lazeyras, F.; Salomir, R.; Polidori, A.; Contino-Pépin, C.; et al. Perfluorocarbon Nanodroplets Stabilized by Fluorinated Surfactants: Characterization and Potentiality as Theranostic Agents. *J. Mater. Chem. B* **2015**, *3* (14), 2892–2907. https://doi.org/10.1039/C4TB01578A.

(16) Fernandes, D. A.; Fernandes, D. D.; Li, Y.; Wang, Y.; Zhang, Z.; Rousseau, D.; Gradinaru, C. C.; Kolios, M. C. Synthesis of Stable Multifunctional Perfluorocarbon Nanoemulsions for Cancer Therapy and Imaging. *Langmuir* **2016**, *32* (42), 10870–10880. https://doi.org/10.1021/acs.langmuir.6b01867.

(17) Oda, Y.; Suzuki, R.; Mori, T.; Takahashi, H.; Natsugari, H.; Omata, D.; Unga, J.; Uruga, H.; Sugii, M.; Kawakami, S.; et al. Development of Fluorous Lipid-Based Nanobubbles for Efficiently Containing Perfluoropropane. *Int. J. Pharm.* **2015**, *487* (1–2), 64–71. https://doi.org/10.1016/J.IJPHARM.2015.03.073.

(18) Koda, Y.; Terashima, T.; Sawamoto, M. Fluorinated Microgel Star Polymers as Fluorous Nanocapsules for the Encapsulation and Release of Perfluorinated Compounds. *Polym. Chem.* **2015**, *6* (31), 5663–5674. https://doi.org/10.1039/c5py00113g.

(19) Houvenagel, S.; Picheth, G.; Dejean, C.; Brulet, A.; Chenneviere, A.; Couture, O.; Huang, N.; Moine, L.; Tsapis, N. End-Chain Fluorination of Polyesters Favors Perfluorooctyl Bromide Encapsulation into Echogenic PEGylated Nanocapsules. *Polym. Chem.* **2017**, *8* (16), 2559–2570. https://doi.org/10.1039/C7PY00400A.

(20) Houvenagel, S.; Moine, L.; Picheth, G.; Dejean, C.; Brûlet, A.; Chennevière, A.; Faugeras, V.; Huang, N.; Couture, O.; Tsapis, N. Comb-Like Fluorophilic-Lipophilic-Hydrophilic Polymers for Nanocapsules as Ultrasound Contrast Agents. *Biomacromolecules* **2018**, *19* (8), 3244–3256. https://doi.org/10.1021/acs.biomac.8b00506.

(21) Kaberov, L. I.; Verbraeken, B.; Hruby, M.; Riabtseva, A.; Kovacik, L.; Kereïche, S.; Brus, J.; Stepanek, P.; Hoogenboom, R.; Filippov, S. K. Novel Triphilic Block Copolymers Based on Poly(2-Methyl-2-Oxazoline)– Block –poly(2-Octyl-2-Oxazoline) with Different Terminal Perfluoroalkyl Fragments: Synthesis and Self-Assembly Behaviour. *Eur. Polym. J.* **2017**, *88*, 645–655. https://doi.org/10.1016/j.eurpolymj.2016.10.016.

(22) Kaberov, L. I.; Verbraeken, B.; Riabtseva, A.; Brus, J.; Talmon, Y.; Stepanek, P.; Hoogenboom, R.; Filippov, S. K. Fluorinated 2-Alkyl-2-Oxazolines of High Reactivity: Spacer-Length-Induced Acceleration for Cationic Ring-Opening Polymerization As a Basis for Triphilic Block Copolymer Synthesis. *ACS Macro Lett.* **2018**, *7* (1), 7–10. https://doi.org/10.1021/acsmacrolett.7b00954.

(23) Riabtseva, A.; Kaberov, L. I.; Noirez, L.; Ryukhtin, V.; Nardin, C.; Verbraeken, B.; Hoogenboom, R.; Stepanek, P.; Filippov, S. K. Structural Characterization of Nanoparticles Formed by Fluorinated Poly(2-Oxazoline)-Based Polyphiles. *Eur. Polym. J.* **2018**, *99*, 518–527. https://doi.org/10.1016/J.EURPOLYMJ.2018.01.007.

(24) Kaberov, L. I.; Verbraeken, B.; Riabtseva, A.; Brus, J.; Radulescu, A.; Talmon, Y.; Stepanek, P.; Hoogenboom, R.; Filippov, S. K. Fluorophilic–Lipophilic–Hydrophilic Poly(2-Oxazoline) Block Copolymers as MRI Contrast Agents: From Synthesis to Self-Assembly. *Macromolecules* **2018**, *51* (15), 6047–6056. https://doi.org/10.1021/acs.macromol.8b00957.

(25) Horváth, I. T. Fluorous Biphase Chemistry. *Acc. Chem. Res.* **1998**, *31* (10), 641–650. https://doi.org/10.1021/ar970342i.

(26) Koda, Y.; Terashima, T.; Sawamoto, M.; Maynard, H. D. Amphiphilic/Fluorous Random Copolymers as a New Class of Non-Cytotoxic Polymeric Materials for Protein Conjugation. *Polym. Chem.* **2015**, *6*, 240–247. https://doi.org/10.1039/C4PY01346H.

(27) Singh, A.; Naskar, A. K.; Haynes, D.; Drews, M. J.; Smith, D. W. Synthesis, Characterization and Surface Properties of Poly(Lactic Acid)-Perfluoropolyether Block Copolymers. *Polym. Int.* **2011**, *60* (3), 507–516. https://doi.org/10.1002/pi.2982.

(28) Giuntoli, G.; Rosi, L.; Frediani, M.; Sacchi, B.; Frediani, P. Fluoro-Functionalized PLA Polymers as Potential Water-Repellent Coating Materials for Protection of Stone. *J. Appl. Polym. Sci.* **2012**, *125* (4), 3125–3133. https://doi.org/10.1002/app.36469.

(29) Diou, O.; Fattal, E.; Delplace, V.; Mackiewicz, N.; Nicolas, J.; Mériaux, S.; Valette, J.; Robic, C.; Tsapis, N. RGD Decoration of PEGylated Polyester Nanocapsules of Perfluorooctyl Bromide for Tumor Imaging: Influence of Pre or Post-Functionalization on Capsule Morphology. *Eur. J. Pharm. Biopharm.* **2014**, *87* (1), 170–177. https://doi.org/10.1016/j.ejpb.2013.12.003.

(30) Aguilar, J. A.; Nilsson, M.; Bodenhausen, G.; Morris, G. A. Spin Echo NMR Spectra without J Modulation. *Chem. Commun.* **2012**, *48* (6), 811–813. https://doi.org/10.1039/C1CC16699A.

(31) Henderson, T. J. Quantitative NMR Spectroscopy Using Coaxial Inserts Containing a Reference Standard: Purity Determinations for Military Nerve Agents. *Anal. Chem.* **2002**, *74* (1), 191–198. https://doi.org/10.1021/ac010809+.

(32) Böhmer, M. R.; Schroeders, R.; Steenbakkers, J. A. M.; de Winter, S. H. P. M.; Duineveld, P. A.; Lub, J.; Nijssen, W. P. M.; Pikkemaat, J. A.; Stapert, H. R. Preparation of Monodisperse Polymer Particles and Capsules by Ink-Jet Printing. *Colloids Surfaces A Physicochem. Eng. Asp.* **2006**, *289* (1–3), 96–104. https://doi.org/10.1016/J.COLSURFA.2006.04.011.

(33) Agrawal, A.; Saran, A. D.; Rath, S. S.; Khanna, A. Constrained Nonlinear Optimization for Solubility Parameters of Poly(Lactic Acid) and Poly(Glycolic Acid) - Validation and Comparison. *Polymer (Guildf).* **2004**, *45* (25), 8603–8612. https://doi.org/10.1016/j.polymer.2004.10.022.

(34) Foster, T.; Dorfman, K. D.; Ted Davis, H. Giant Biocompatible and Biodegradable PEG–PMCL Vesicles and Microcapsules by Solvent Evaporation from Double Emulsion Droplets. *J. Colloid Interface Sci.* **2010**, *351* (1), 140–150. https://doi.org/10.1016/J.JCIS.2010.05.020.

(35) Berger, R.; Resnati, G.; Metrangolo, P.; Weber, E.; Hulliger, J. Organic Fluorine

Compounds: A Great Opportunity for Enhanced Materials Properties. *Chem. Soc. Rev.* **2011**, *40* (7), 3496. https://doi.org/10.1039/c0cs00221f.

(36) Ojogun, V.; Knutson, B. L.; Vyas, S.; Lehmler, H.-J. Fluorophilicity of Alkyl and Polyfluoroalkyl Nicotinic Acid Ester Prodrugs. *J. Fluor. Chem.* **2010**, *131* (7), 784–790. https://doi.org/10.1016/J.JFLUCHEM.2010.04.001.

(37) Shen, J.; Piunova, V. A.; Nutt, S.; Hogen-Esch, T. E. Blends of Polystyrene and Poly(n-Butyl Methacrylate) Mediated by Perfluorocarbon End Groups. *Polymer (Guildf).* **2013**, *54* (21), 5790–5800. https://doi.org/10.1016/J.POLYMER.2013.08.059.

(38) Marchione, A. A.; Buck, R. C. Complete Multinuclear Magnetic Resonance Characterization of a Set of Polyfluorinated Acids and Alcohols. *Magn. Reson. Chem.* **2009**, *47* (2), 194–198. https://doi.org/10.1002/mrc.2376.

(39) Twum, E. B.; Gao, C.; Li, X.; McCord, E. F.; Fox, P. A.; Lyons, D. F.; Rinaldi, P. L. Characterization of the Chain-Ends and Branching Structures in Polyvinylidene Fluoride with Multidimensional NMR. *Macromolecules* **2012**, *45* (13), 5501–5512. https://doi.org/10.1021/ma300835s.

(40) Kadayakkara, D. K.; Damodaran, K.; Hitchens, T. K.; Bulte, J. W. M.; Ahrens, E. T. 19F Spin–lattice Relaxation of Perfluoropolyethers: Dependence on Temperature and Magnetic Field Strength (7.0–14.1 T). *J. Magn. Reson.* **2014**, *242*, 18–22. https://doi.org/10.1016/J.JMR.2014.01.014.

(41) Chung, T.-W.; Huang, Y.-Y.; Liu, Y.-Z. Effects of the Rate of Solvent Evaporation on the Characteristics of Drug Loaded PLLA and PDLLA Microspheres. *Int. J. Pharm.* **2001**, *212* (2), 161–169. https://doi.org/10.1016/S0378-5173(00)00574-3.

(42) Lebedeva, N. V.; Sanders, S. N.; Ina, M.; Zhushma, A. P.; Olson, S. D.; Rubinstein, M.; Sheiko, S. S. Multicore Expandable Microbubbles: Controlling Density and Expansion Temperature. *Polymer (Guildf).* **2016**, *90*, 45–52. https://doi.org/10.1016/J.POLYMER.2016.02.050.